Batteries & Supercaps

Research Article
doi.org/10.1002/batt.202200152

Chemistry Europe
European Chemical Societies Publishing

www.batteries-supercaps.org

Glyoxal-Based Electrolytes in Combination with Fe_2O_3@C-Based Electrodes for Lithium-Ion Batteries

Annika Bothe,[a] Lydia Gehrlein,[b] Qiang Fu,[b] Chengping Li,[b, c] Julia Maibach,[b] Sonia Dsoke,*[b] and Andrea Balducci*[a]

In this study, we report for the first time about using glyoxal-based electrolytes in combination with a Fe_2O_3@C-based conversion type anode for application in lithium-ion batteries (LIBs). We show that at room temperature (RT) the use of these alternative electrolytes is possible, but it is not more advantageous than that of the conventional LP30. At 60 °C, on the other hand, utilizing a glyoxal-based electrolyte appears very promising since the Fe_2O_3@C-based electrode, cycled in combination with 1 M LiTFSI in TEG:PC + 2% VC, displays a high specific capacity (800 mAh g^{-1}) and a high stability over 500 cycles. X-ray photoelectron spectroscopy (XPS) measurements indicate that these high performances are possible thanks to the generation of a thermally stable and thick SEI, which is particularly favorable for maintaining a highly reversible conversion reaction.

Introduction

Lithium-ion batteries (LIBs) are nowadays the most important and widespread energy storage devices in our society and they are used in many applications, ranging from portable devices to transportation.[1] The success of LIBs is related to their high specific energy, high specific power, and high cycling stability, which make them suitable for applications such as in electric vehicles and electric grid as well as off-grid power supply systems, that are challenging, or even not possible, for other energy storage technologies.[1a,2]

The state-of-the-art LIB contains a graphite anode, a lithium metal oxide cathode (e.g., NMC), and an electrolyte consisting of a mixture of linear and cyclic carbonates, e.g., ethylene carbonate (EC) and dimethyl carbonate (DMC), in which lithium hexafluorophosphate ($LiPF_6$) is dissolved.[1c,2a,3] This electrode-electrolyte combination enables the favorable properties mentioned above. However, it has been widely shown that replacing graphite with a high-capacity anodic material and substituting the organic carbonates with less flammable and more thermally stable electrolytes could significantly improve the energy density and the safety of LIBs.[3b,4] This overall improvement is considered of key importance for the widespread application of LIBs in electric vehicles, which is indispensable for a complete transition from combustions engines to electromobility.[1c] For this reason, in the last years, enormous efforts have been made towards the development of alternative electrode materials and electrolytes for LIBs.

Among the alternative anodic materials, transition metal oxides (TMOs), which include TMOs based on many different elements (e.g., manganese,[5] chromium,[6] iron,[7] tin[8] and cobalt[9]), are considered of great interest due to their high theoretical capacity. Fe_2O_3 is considered one of the most promising materials belonging to this category due to its low toxicity, low cost, and high theoretical capacity (1007 mAh g^{-1}).[7a,10] The conversion reaction involving Fe_2O_3 leads to the complete reduction of the transition metal [Fe(III)) to its metallic state (Fe)], which involves up to six electrons [see Equation (1)].[10,11]

$$Fe_2O_3 + 6\ Li^+ + 6e^- \rightleftharpoons 2Fe + 3\ Li_2O \quad (1)$$

Although very attractive, electrodes based on Fe_2O_3 typically suffer from low cycling stability due to the large volume changes taking place during the charge-discharge process and do not display high performance at high C-rates due to their low electronic conductivity.[7a,11] To overcome these limitations, many different nanostructures of controlled particle size, morphology, and composition have been introduced.[11,12] This includes e.g., hollow nanostructures derived from metal-organic frameworks (MOFs),[7a,13] nanorods,[14] nanoflakes,[15] and

[a] A. Bothe, Prof. A. Balducci
Friedrich-Schiller-University Jena
Institute for Technical Chemistry and Environmental Chemistry
Center for Energy and Environmental Chemistry Jena (CEEC Jena)
Philosophenweg 7a, 07743 Jena, Germany
E-mail: andrea.balducci@uni-jena.de
[b] L. Gehrlein, Q. Fu, C. Li, J. Maibach, S. Dsoke
Karlsruhe Institute of Technology (KIT)
Institute for Applied Materials (IAM)
Hermann-von-Helmholtz-Platz 1, 76344 Eggenstein-Leopoldshafen, Germany
E-mail: sonia.dsoke@kit.edu
[c] C. Li
Faculty of Materials Science and Engineering
Kunming University of Science and Technology
Kunming 650093, China

Supporting information for this article is available on the WWW under https://doi.org/10.1002/batt.202200152

An invited contribution to a Special Collection dedicated to the 5-Year Anniversary of Batteries & Supercaps

nanocomposite material.[16] Recently, electrodes based on core-shell Fe_2O_3@C nanospheres displayed high capacity and stability in LIBs, paving the way to realize high-performance electrodes.[7a,13a]

Concerning alternative electrolytes, those based on glyoxal solvents, e.g., 1,2,2-tetraethoxyethane (TEG) and 1,1,2,2-tetramethoxyethane (TMG), are nowadays regarded with increasing attention. As a matter of fact, these solvents are largely available (they are already produced in the multi-ton scale), making them cheap and they display low melting and high flash points, high thermal stability, and favorable transport properties.[17] In the last years, it has been shown that they can be successfully utilized in LIBs and potassium-ion batteries (PIBs), and that their use is advantageous at room temperature (RT) as well as at elevated temperatures.[17b,e,18]

Considering the favorable features of core-shell Fe_2O_3@C nanospheres and glyoxal-based electrolytes, their combination could have a positive impact on the performance and safety of LIBs. To the best of our knowledge, however, this electrode-electrolyte combination has not been considered so far. Therefore in this study, we investigate the electrochemical performance of electrodes containing Fe_2O_3@C nanospheres in different TEG-based electrolytes at RT and 60 °C, and compare the results to those obtained in the conventional electrolyte LP30. To have a better understanding about the interaction between these electrolytes with the anode material, the electrochemical characterization is complemented with XPS analyses focusing on the SEI composition.

Experimental Section

Electrolyte preparation

1,1,2,2-Tetraethoxyethane (TEG, WeylChem) was purified by an overpressure filtration over dried aluminum oxide to reduce the water content ($\leq$ 20 ppm, determined by Karl-Fischer titration, C20 Mettler Toledo) and to remove any stabilizer. Propylene carbonate (PC, Sigma Aldrich) and 1 M $LiPF_6$ in ethylencarbonate (EC) : dimethylcarbonate (DMC) (1:1) (LP30, Solvionic) were used as received. Lithium bis(trifluoromethanesulfonyl)imide (LiTFSI, Solvionic) was used without any further purification. The additive vinylene carbonate (VC, 98%, Arcos Organics) was stored in a freezer until use. The electrolytes were prepared in an argon-filled glovebox (MBraun, O_2 and $H_2O < 1$ ppm). Three electrolytes were used for the investigations reported in this work: LP30 (used as received), 1 M LiTFSI in TEG + 2 wt% VC and 1 M LiTFSI in TEG:PC (3:7, wt) + 2 wt% VC. For sake of simplicity, in the following, these electrolytes will be indicated as LP30, TEG-2VC, and TEG:PC-2VC, respectively.

Electrode preparation

Composite electrodes containing Fe_2O_3@C nanospheres as the active material were prepared following a procedure identical to that described in our previous work.[7a] The electrode composition was: 70 wt% Fe_2O_3@C nanospheres, 20 wt% conducting agent (Super P, Timcal Ltd.) and 10 wt% binder [sodium alginate, Sigma Aldrich, 3% sodium alginate in deionized water:isopropanol (9:1) as solvent]. The slurry was mechanically stirred for 12 h and coated on copper foil. Circular electrodes with a diameter of 12 mm were punched out and dried at 80 °C in a vacuum oven for 24 h. The average active electrode mass was 1.15 mg ± 0.2 mg and the electrode area was 1.13 cm^2.

Electrochemical measurements

The electrochemical measurements were carried out utilizing a Swagelok type 3-electrode set up, assembled in a glovebox. The Fe_2O_3@C-based electrodes were used as working electrode, while lithium metal was used as counter and reference electrodes. The electrodes were separated by a Whatman GF/D glass microfiber filter drenched with 120 µL of electrolyte.

Electrochemical tests have been performed using a VMP III multichannel potentiostatic-galvanostatic system (Biologic Science Instruments) and a LBT21084 multichannel potentiostatic-galvanostatic system (Arbin Instruments). Cyclic voltammetry (CV) was carried out utilizing a scan rate of 0.05 mV s^{-1}. Galvanostatic charge and discharge (GCD) at different C-rates, related to the theoretical capacity of Fe_2O_3 (0.1 C, 0.2 C, 0.5 C, 1 C, 2 C and 4 C) followed by prolonged charge-discharge (500 cycles at 0.5 C) have been carried out to evaluate the electrochemical performance of the electrodes. The voltage range was set to 0.01–3 V vs. Li^+/Li for all the measurements, which have been carried out at room temperature (RT) and 60 °C (using an oven, Binder).

XPS measurements

All samples were washed by a 1-minute submersion in 1 ml dimethyl carbonate (DMC). After washing, all electrodes were dried and mounted on a sample holder using conductive copper tape. The sample preparation was carried out in an argon-filled glove box (H_2O & $O_2 < 1$ ppm). Transfer to the XP spectrometer was done via a transfer module under inert gas conditions. To ensure potential stability, the delithiation endpoint potentials were held for 1 h after the electrochemical cycling. XPS measurements were carried out with a K-alpha spectrometer from Thermo-Fisher Scientific applying a micro-focused, monochromated Al-K_α x-ray source with 400 µm spot size. A pass energy of 50 eV was used. Data acquisition and handling were done via the Thermo Avantage software by K.L. Parry et al.[19] Spectra were fitted with one or more Voigt profiles and Scofield sensitivity factors were applied for quantification. All spectra were referenced in binding energy to the hydrocarbon C 1s peak at 285 eV. For clarity of presentation, all spectra were normalized in intensity to the maximum intensity (i.e., highest peak and background were normalized in intensity to [1,0]).

Results and Discussion

Fe_2O_3@C hollow nanospheres contain two phases of Fe_2O_3 (*Fd* $\bar{3}m$, 73 wt% and *R*$\bar{3}c$, 27 wt%), and 28.4 wt% of carbon, as reported in our previous work.[7a] The unique hollow and porous structure can not only increase the interaction between the active material and the electrolyte, but also alleviate the mechanical strains during cycling. Moreover, the amorphous carbon coating on the surface of Fe_2O_3 provides good electronic conductivity. As reported in our previous work, Fe_2O_3@C hollow nanospheres show a high initial capacity with more than 1000 mAh g^{-1} at 100 mA g^{-1} in both LP30 and LiTFSI-EC-DMC electrolytes at RT, demonstrating its great potential as anode material for LIBs.

Research Article
doi.org/10.1002/batt.202200152
Chemistry Europe
European Chemical Societies Publishing

Table 1 compares the viscosities and conductivities of the three electrolytes (without VC additive) investigated in this study at 20 °C and 60 °C. At these temperatures, the conductivity and viscosity of the TEG-2VC electrolyte are not as favorable as those of the state-of-the-art electrolyte LP30. Adding PC improves the transport properties of the electrolytic solution, but the conductivity and viscosity of TEG:PC-2VC are still not reaching those of LP30. Nonetheless, as already reported, the transport properties of the two glyoxal electrolytes are suitable for their use in LIBs, and both guarantee good performance in a broad range of C-rates.[17b,e] Not to forget that electrolytes based on TEG display higher thermal stability, lower vapor pressure, and higher boiling points compared to LP30.[17b,d]

Figure 1 shows the evolution of the specific capacity of the Fe_2O_3@C electrodes over 500 cycles at RT and 60 °C with a C-rate of 0.5 C. Before starting the cycling process, a C-rate test was performed for all electrodes (see Experimental Section and Figure S1 in Supporting Information). At RT (Figure 1a), electrodes show comparable initial capacities in all 3 electrolytes. The electrodes cycled in the two glyoxal-based electrolytes show an initial decrease in specific capacity, but after approx. 100 cycles, their capacity stabilizes and it is equal to ca. 280 mAh g^{-1} at the end of cycling. The electrode cycled in LP30 shows a different behavior. Also, this electrode shows a decrease in capacity over the first 100 cycles, followed by an increase and a subsequent stabilization after 200 cycles at a value of ca. 500 mAh g^{-1}. This behavior was already observed in our previous work,[7a] which attributes it to a modification of the SEI over the cycling process. In all electrolytes, the efficiency of the charge-discharge process is close to 100% for all cycles. A completely different behavior is observed when the cycling process is performed at 60 °C (Figure 1b). In this case, the electrode cycled in TEG-2VC shows a stable behavior over 500 cycles, but its capacity (ca. 180 mAh g^{-1}) is lower compared to that observed at RT. The electrode cycled in LP30 exhibits a decrease of specific capacity during the first 50 cycles, followed by a constant capacity increase and after 500 cycles, a capacity of 355 mAh g^{-1} is reached. The capacity decrease during the first 50 cycles is also observed when the electrode is used in combination with TEG:PC-2VC. However, afterwards, the electrode capacity increases markedly and after 500 cycles, a capacity of 815 mAh g^{-1} is achieved, which is close to the theoretical capacity of this material. To the best of our knowledge, this is one of the best values of capacity stability (after 500 cycles) reported so far for a Fe_2O_3-based electrode cycled at 60 °C. The effect of capacity variation over cycling has been reported several times in literature for electrodes based on conversion materials like the one considered in this study. The decrease of capacity is attributed primarily to changes in the SEI, due to the large volumetric expansion/contraction that these electrodes undergo during the charge-discharge process, and to the formation of compounds, e.g., cubic $LiFeO_2$, which display lower specific capacity than the initial Fe_2O_3.[5a,c,7b,9c,11,21] The increase in capacity, on the other hand, is often justified by the formation of isolated metallic nanograins, which promote the formation of a polymeric gel-like film that enhances lithium storage as well as the activation of the porous structures.[5c,11,21b,c,e–h,22] Taking the results of Figure 1 into account, it seems that using TEG:PC-2VC at 60 °C creates a very favorable environment for the Fe_2O_3@C electrodes, which allows them to exploit almost all their theoretical capacity over a large number of charge-discharge cycles. CV measurements (Supporting Information Figure S2) show that when cycling in the TEG:PC-2VC electrolyte at 60 °C, a peak emerges at 1.41 V in the first cycle, which is not observed with the other electrolytes

Table 1. Transport properties of the selected electrolytes at 20 °C and 60 °C.

	Viscosity [mPa s]		Conductivity [mS cm^{-1}]	
	20 °C	60 °C	20 °C	60 °C
1 M LiTFSI in TEG[17e]	11.0	4.1	1.5	3.5
1 M LiTFSI in TEG:PC (3:7)[17e]	8.6	3.7	3.5	7.9
LP30[20]	~5.5	~2.0	~10.5	~19.5

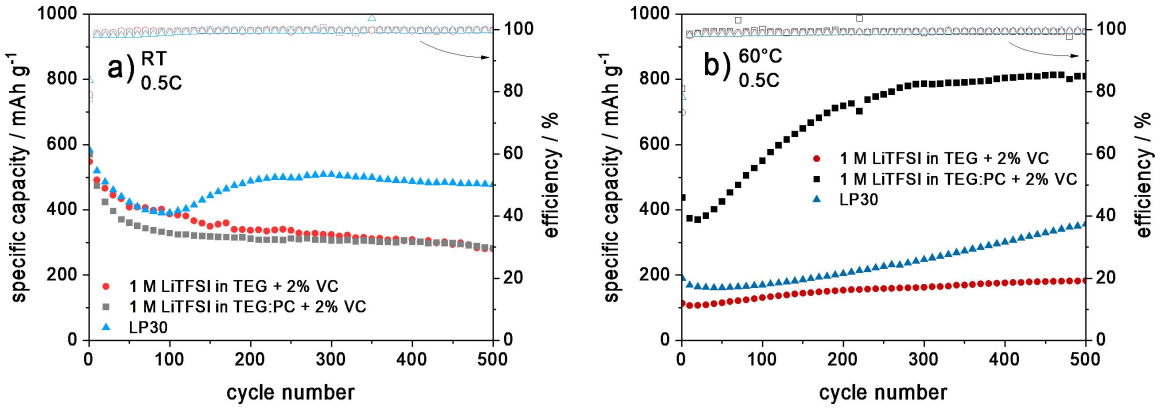

Figure 1. Cycling stability (at 0.5 C) of Fe_2O_3@C electrodes in TEG-2VC, TEG:PC-2VC and LP30 at: a) RT and b) 60 °C.

Research Article
doi.org/10.1002/batt.202200152
Chemistry Europe
European Chemical Societies Publishing

and might indicate thicker SEI formation (Supporting Information Figure S2d).

Figure 2 compares the evolution of selected charge and discharge profiles (cycles 10, 250 and 500) at RT and at 60 °C. During the first cycles at RT, a short plateau at ca. 1.0 V vs. Li^+/Li is displayed by all electrodes, which can be attributed to the conversion reaction [Fe(III) to Fe(0)].[7a] Throughout the cycling process, the plateau disappears in all electrolytes. However, while the capacity of the electrodes cycled in the glyoxal-based electrolytes decreases (see Figure 3a and b), the one of the electrode cycled in LP30 is maintained. In this latter case, the discharge profile becomes more slopy indicating a charge storage and delivery over a range of potentials.[11] At 60 °C, the situation is completely different. The electrode cycled in TEG-2VC does not show any plateau at the beginning of the cycling process, but only a slopy profile, which is maintained during all cycles, as provided capacity. The electrode cycled in LP30 displays a slopy profile at the beginning of the cycling process, and its discharge profile is rather comparable to that observed in TEG-2VC. However, during cycling, the profile changes and after 500 cycles, a small plateau at ca. 1.0 V vs. Li^+/Li appears. The presence of this plateau corresponds to the increase in electrode capacity. A similar behavior is also displayed by the electrode cycled in TEG:PC-2VC. However, in this case, the initial capacity is higher than that observed in LP30 (400 mAh g^{-1} vs. 150 mAh g^{-1}) and the plateau, which appears during the

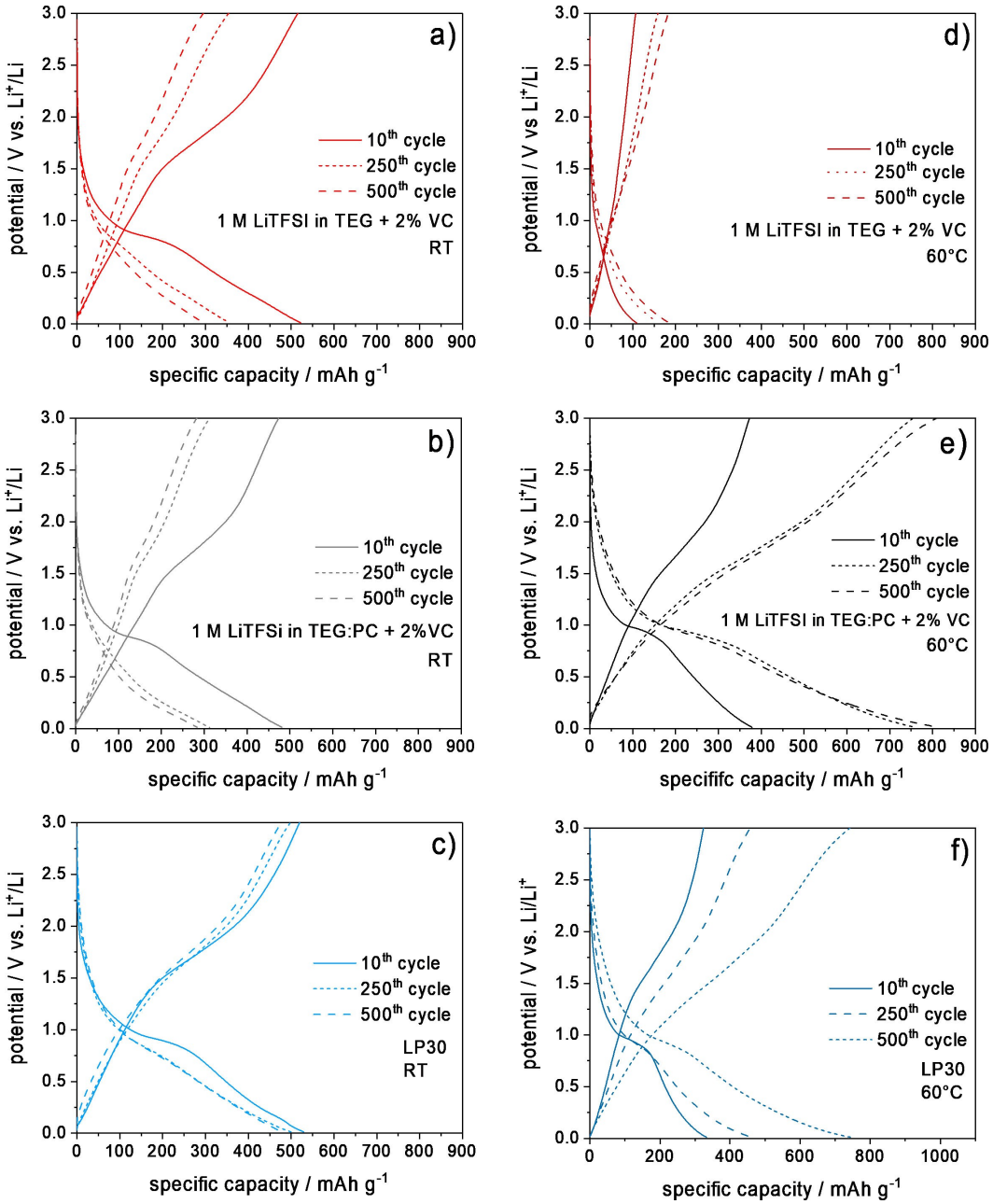

Figure 2. Charge and discharge profiles (at 0.5 C) of Fe_2O_3@C electrodes at RT and 60 °C in: a, d) TEG-2VC, b, e) TEG:PC-2VC and c, f) LP30.

Research Article
doi.org/10.1002/batt.202200152
Chemistry Europe
European Chemical Societies Publishing

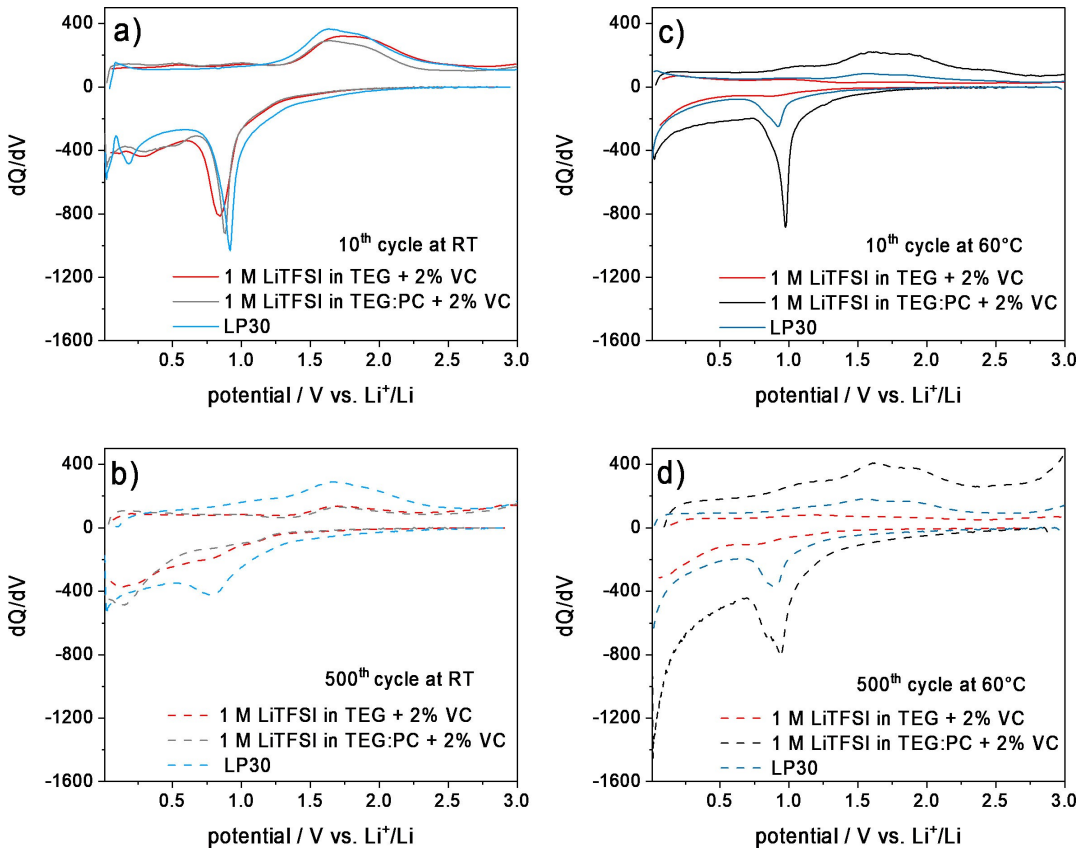

Figure 3. Evolution of the differential specific capacity of the of Fe_2O_3@C electrodes (10th and 500th cycles) in the electrolytes TEG-2VC, TEG:PC-2VC and LP30 at a, b) RT and c, d) 60 °C.

cycling process, is significantly larger than that observed in the conventional electrolyte. As a consequence, the capacity delivered by the electrode cycled in TEG:PC-2VC increases, till the 250th cycle, to a value of 800 mAh g^{-1}. This value, which is the double of that observed in LP30, is maintained for the following cycles, until the 500th cycle. During this large number of cycles, the efficiency of the charge-discharge process is always close to 100 % ($\emptyset$ = 99.5 %), indicating that the use of TEG:PC-2VC at 60 °C is establishing an environment in which the Fe_2O_3@C electrodes can reversibly deliver very high capacity.

The establishment of this favorable environment at 60 °C is also well visible in the evolution of the differential capacity of the electrode during the cycling process. As shown in Figure 3, at RT, the peak at 1.0 V vs. Li^+/Li, which is assigned to the conversion reaction of Fe(III) to Fe(0), disappears completely in the electrodes cycled in the two glyoxal-based electrolytes. In contrast, when LP30 is used, the peak is only partially disappearing, explaining the higher capacity observed in this electrolyte discussed above. At 60 °C, the peak at 1.0 V vs. Li^+/Li is never observed in the electrolyte TEG-2VC, explaining the low and constant capacity delivered by the electrode (see discussion above). On the contrary, in the electrolytes LP30 and TEG:PC-2VC, the peak at 1.0 V vs. Li^+/Li is visible through the entire cycling process. In the case of TEG:PC-2VC, however, also an increase of the capacity at potentials below 1.0 V vs. Li^+/Li is taking place, which represents an important contribution to the total electrode capacity.

XPS is employed to analyze the effect of the respective electrolyte formulations on SEI properties of Fe_2O_3@C electrodes. Figures 4 and 5 show the C1s and F1s spectra of Fe_2O_3@C electrodes stored at open-circuit voltage (OCV) for two hours at RT and at 60 °C in the respective electrolyte TEG:PC-2VC and LP30. Also shown are the spectra after 5 cycles. Four peaks are observed in the C1s spectra of Fe_2O_3@C electrodes stored in TEG:PC-2VC-RT, LP30-RT, and LP30-60 °C, see Figure 4 (a and b): sp^2 hybridized carbon of the carbon black conductive additive (284.2 eV), adventitious carbon (285 eV), and the two chemical environments of the carboxymethyl cellulose (CMC) binder –C–O–C– (286.5 eV) and $–CO_2$ (289.1 eV). By contrast, the electrode stored in TEG:PC-2VC at 60 °C displays typical SEI compounds resulting from PC and TEG decomposition products: hydrocarbons (285 eV), –C–O (286.5 eV), $–CO_2Li$ (289.0 eV), and $–CO_3Li$ (290.0 eV). Two additional peaks emerge at 287.6 eV and 291.0 eV, corresponding to the two chemical environments C_a and C_b in poly(VC). Poly(VC) originates from the decomposition of the electrolyte additive vinylene carbonate (VC).[23] Similar SEI species are observed after 5 cycles in the TEG:PC-2VC electrolyte formulation at RT and 60 °C. The built-up of an SEI layer is also seen in the intensity decrease of the sp^2 peak. After cycling in the LP30 electrolyte, C1s spectra at RT and 60 °C show EC and DMC decomposition products:

Research Article
doi.org/10.1002/batt.202200152
Chemistry Europe
European Chemical Societies Publishing

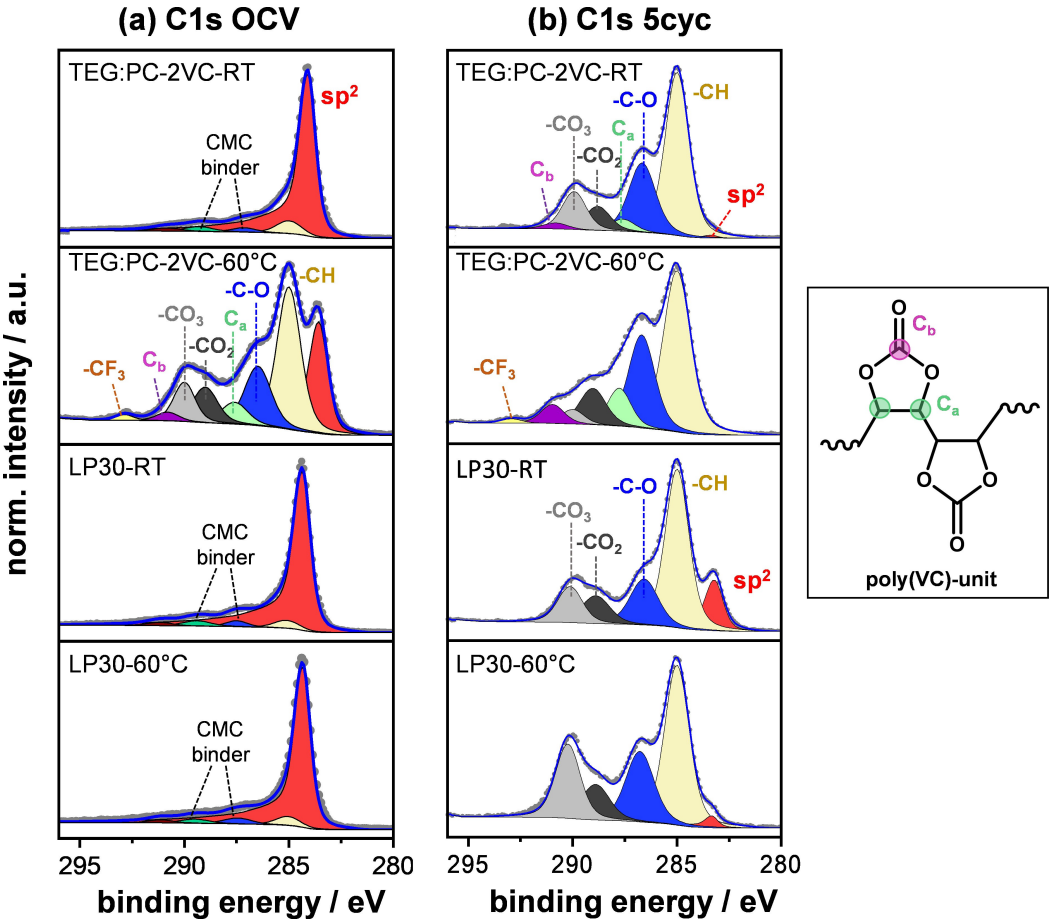

Figure 4. a) C1s photoelectron spectra of Fe_2O_3@C electrodes at OCV stage in TEG:PC-2VC and LP30 electrolytes at RT and 60 °C, b) C1s spectra after 5 cycles in TEG:PC-2VC and LP30 electrolytes at RT and 60 °C.

hydrocarbons (285 eV), –C–O (286.5 eV), $–CO_2Li$ (288.9 eV), and $–CO_3Li$ (290.1 eV). F1s spectra of Figure 5(a and b) displays two peaks when cycling in the TEG:PC-2VC electrolyte: LiF (685 eV) resulting from LiTFSI decomposition and $–CF_3$ groups (693.3 eV) of the LiTFSI electrolyte salt. Electrodes stored at OCV and cycled in LP30 display two peaks that can be ascribed to $LiPF_6$ decomposition products LiF (684.9 eV) and Li_xPF_y/$Li_xPF_yO_z$ (~687.5 eV). The presence of LiF during OCV storage indicates that both LiTFSI and $LiPF_6$ already decompose to a small degree before cycling. The increase in temperature from RT to 60 °C leads to overall more electrolyte decomposition, as it can be seen in an increase in peak intensities and atomic percentages (Figures 4 and 5, Tables 2 and 3). When comparing the SEI composition of LP30 to TEG:PC-2VC, more $–CO_3Li$ and LiF are observed at RT and 60 °C on electrodes cycled in LP30. While an increase in detected $–CO_3Li$ species is related to

Table 2. Atomic percentages of selected SEI species –C–O, $–CO_3$, and LiF of Fe_2O_3@C electrodes in TEG:PC-2VC and LP30 after storage in OCV at RT and 60 °C.

Species	TEG:PC-2VC		LP30	
	OCV_RT	OCV_60 °C	OCV_RT	OCV_60 °C
–C–O	0	7.12	0	0
$–CO_3$	0	3.78	0	0
LiF	0.66	0.94	0.77	0.61

Table 3. Atomic percentages of selected SEI species –C–O, $–CO_3$ and LiF of Fe_2O_3@C electrodes in TEG:PC-2VC and LP30 after 5 cycles at RT and 60 °C.

Species	TEG:PC-2VC		LP30	
	5cyc_RT	5cyc_60 °C	5cyc_RT	5cyc_60 °C
–C–O	10.58	12.71	6.33	7.35
$–CO_3$	3.76	1.72	4.36	6.79
LiF	0.53	0.61	2.57	4.21

Research Article
doi.org/10.1002/batt.202200152
Chemistry Europe
European Chemical Societies Publishing

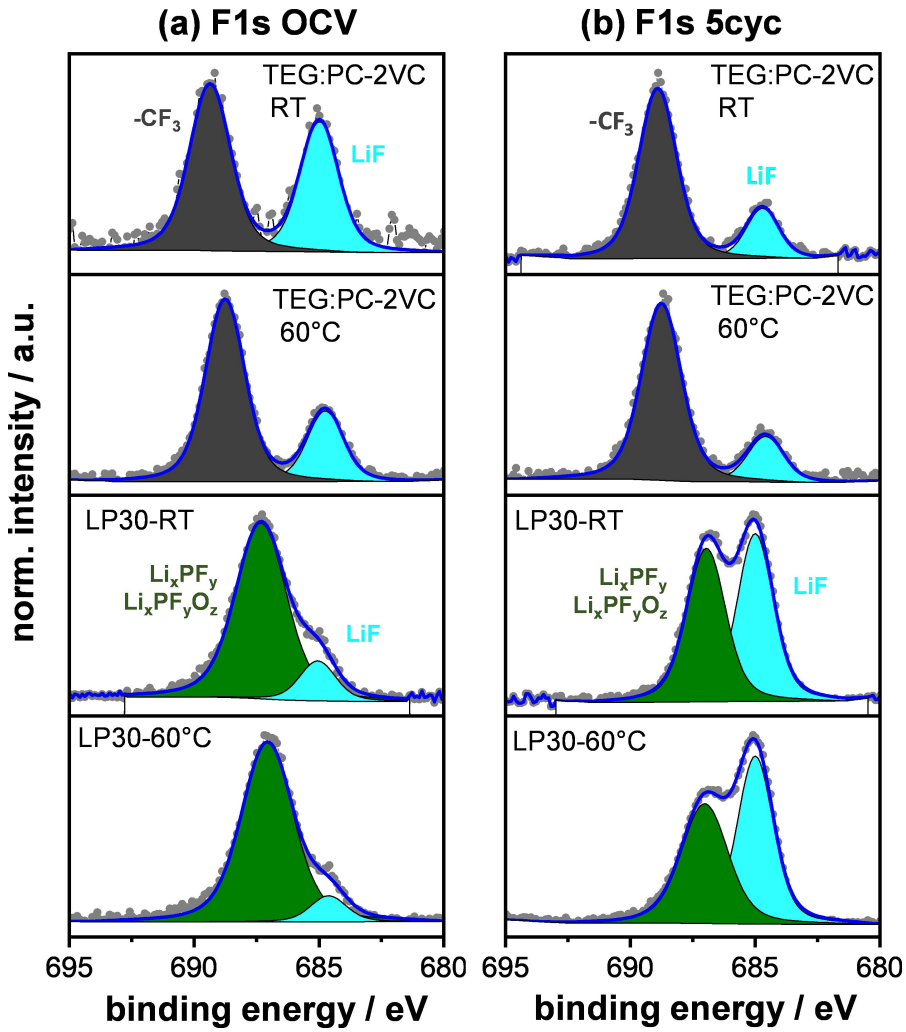

Figure 5. a) F1s photoelectron spectra of Fe_2O_3@C electrodes at RT and 60 °C, b) F1s spectra after 5 cycles in TEG:PC-2VC and LP30 electrolytes at RT and 60 °C.

higher EC decomposition, higher LiF content results from the low thermal stability of LP30 at elevated temperatures. While this is only a comparison after 5 cycles, an increase in EC and $LiPF_6$ decomposition could also occur at later cycling stages. This could explain the poor electrochemical performance of Fe_2O_3@C electrodes in LP30 at elevated temperatures. In contrast, TEG:PC-2VC leads to an SEI at both RT and 60 °C, which is primarily composed of hydrocarbons, –C–O compounds, and poly(VC). Also, very little LiTFSI salt decomposition (i.e., LiF) is observed. This SEI composition seems to be more favorable at elevated temperatures.

Conclusion

In this work, we report for the first time about using Fe_2O_3@C-based electrodes in combination with glyoxal-based electrolytes. We show that at RT the use of these alternative electrolytes is possible, but not more advantageous than that of the conventional LP30. At 60 °C, on the other hand, the use of glyoxal-based electrolytes appears very promising. As illustrated, at this temperature, the Fe_2O_3@C-based electrode cycled with TEG:PC-2VC displays high specific capacity (800 mAh g^{-1}) and high stability over 500 cycles. To the best of our knowledge, this is one of the best performances reported so far for Fe_2O_3@C-based conversion materials operating at high temperatures. XPS measurements indicate that, in contrast to LP30, less salt decomposition occurs when cycling in TEG:PC-2VC at 60 °C. Also, a smaller amount of carbonates is detected. In fact, using TEG:PC-2VC as an electrolyte, generates an SEI, which is primarily composed of hydrocarbons, –C–O compounds, and poly(VC). Additionally, less LiF decomposition products are observed due to the high thermal stability of LiTFSI. We hypothesize this SEI composition to be more favorable at elevated temperatures.

Considering these results, the combination of glyoxal-PC electrolyte with Fe_2O_3@C-based electrodes appears certainly as very interesting to develop advanced LIBs. In addition to the high values for the capacity, the increased safety of this electrolyte-electrode combination (due to a better thermal stability of conducting salt and solvent) must be emphasized in comparison to the state-of-the-art compounds. These features

make this electrolyte-electrode combination a promising candidate for the realization of advanced LIBs. In the future, it will be important to reduce the number of cycles needed to reach the maximum capacity. A deeper understanding of the SEI formation at different temperatures and tuning the electrolyte formulation appear as two important aspects to reach this goal.

Acknowledgements

A.B. and A.B. wish to thank the Deutsche Forschungsgemeinschaft (DFG) [project BA4956/8-1] for the financial support. C.L. acknowledges the China Scholarship Council (CSC, No.: 201707030004) financial support for pursuing his Ph.D. degree at the Karlsruhe Institute of Technology. This work contributed to the research performed at CELEST (Center for Electrochemical Energy Storage Ulm-Karlsruhe). Open Access funding enabled and organized by Projekt DEAL.

Conflict of Interest

The authors declare no conflict of interest.

Data Availability Statement

The data that support the findings of this study are available from the corresponding author upon reasonable request.

Keywords: conversion-type anode · Fe_2O_3 · glyoxal-based electrolytes · thermal stability

[1] a) G. Zubi, R. Dufo-López, M. Carvalho, G. Pasaoglu, *Renewable Sustainable Energy Rev.* **2018**, *89*, 292–308; b) S. Passerini, D. Bresser, A. Moretti, A. Varzi, *Batteries, 2 Volume Set: Present and Future Energy Storage Challenges*, John Wiley & Sons, **2020**; c) J. Kalhoff, G. G. Eshetu, D. Bresser, S. Passerini, *ChemSusChem* **2015**, *8*, 2154–2175.
[2] a) B. Scrosati, J. Garche, *J. Power Sources* **2010**, *195*, 2419–2430; b) D. Bresser, S. Passerini, B. Scrosati, *Energy Environ. Sci.* **2016**, *9*, 3348–3367.
[3] a) J. Xie, Y.-C. Lu, *Nat. Commun.* **2020**, *11*, 2499; b) M. Armand, P. Axmann, D. Bresser, M. Copley, K. Edström, C. Ekberg, D. Guyomard, B. Lestriez, P. Novák, M. Petranikova, W. Porcher, S. Trabesinger, M. Wohlfahrt-Mehrens, H. Zhang, *J. Power Sources* **2020**, *479*, 228708.
[4] L. Zhao, A. Inoishi, S. Okada, *J. Power Sources Adv.* **2021**, *12*, 100079.
[5] a) Z. Zhao, L. Gehrlein, A. Bothe, J. Maibach, A. Balducci, S. Dsoke, *Energy Technol.* **2021**, *9*, 2100247; b) Z. Zhao, G. Tian, A. Sarapulova, G. Melinte, J. L. Gómez-Urbano, C. Li, S. Liu, E. Welter, M. Etter, S. Dsoke, *ACS Appl. Mater. Interfaces* **2019**, *11*, 29888–29900; c) H. Duncan, F. M. Courtel, Y. Abu-Lebdeh, *J. Electrochem. Soc.* **2015**, *162*, A7110–A7117; d) S. M. Hwang, S. Y. Kim, J.-G. Kim, K. J. Kim, J.-W. Lee, M.-S. Park, Y.-J. Kim, M. Shahabuddin, Y. Yamauchi, J. H. Kim, *Nanoscale* **2015**, *7*, 8351–8355.
[6] Y. Fu, H. Gu, X. Yan, J. Liu, Y. Wang, J. Huang, X. Li, H. Lv, X. Wang, J. Guo, G. Lu, S. Qiu, Z. Guo, *Chem. Eng. J.* **2015**, *277*, 186–193.
[7] a) C. Li, A. Sarapulova, Z. Zhao, Q. Fu, V. Trouillet, A. Missiul, E. Welter, S. Dsoke, *Chem. Mater.* **2019**, *31*, 5633–5645; b) H. Kitaura, K. Takahashi, F. Mizuno, A. Hayashi, K. Tadanaga, M. Tatsumisago, *J. Power Sources* **2008**, *183*, 418–421.
[8] a) H. Xue, J. Zhao, J. Tang, H. Gong, P. He, H. Zhou, Y. Yamauchi, J. He, *Chem. Eur. J.* **2016**, *22*, 4915–4923; b) S. M. Hwang, Y.-G. Lim, J.-G. Kim, Y.-U. Heo, J. H. Lim, Y. Yamauchi, M.-S. Park, Y.-J. Kim, S. X. Dou, J. H. Kim, *Nano Energy* **2014**, *10*, 53–62.
[9] a) B.-M. Chae, E.-S. Oh, Y.-K. Lee, *J. Power Sources* **2015**, *274*, 748–754; b) Q. Lin, Y. Sha, B. Zhao, Y. Chen, M. O. Tadé, Z. Shao, *Electrochim. Acta* **2015**, *180*, 914–921; c) M. Bhardwaj, A. Suryawanshi, R. Fernandes, S. Tonda, A. Banerjee, D. Kothari, S. Ogale, *Mater. Res. Bull.* **2017**, *90*, 303–310; d) D. Puthusseri, V. Aravindan, S. Madhavi, S. Ogale, *Energy Technol.* **2016**, *4*, 816–822.
[10] a) S. Fang, D. Bresser, S. Passerini, *Adv. Energy Mater.* **2020**, *10*, 1902485; b) J. Cabana, L. Monconduit, D. Larcher, M. R. Palacín, *Adv. Mater.* **2010**, *22*, E170–E192.
[11] D. Puthusseri, M. Wahid, S. Ogale, *ACS Omega* **2018**, *3*, 4591–4601.
[12] M. Valvo, F. Lindgren, U. Lafont, F. Björefors, K. Edström, *J. Power Sources* **2014**, *245*, 967–978.
[13] a) C. Li, Q. Hu, Y. Li, H. Zhou, Z. Lv, X. Yang, L. Liu, H. Guo, *Sci. Rep.* **2016**, *6*, 25556; b) X. Xu, R. Cao, S. Jeong, J. Cho, *Nano Lett.* **2012**, *12*, 4988–4991; c) L. Zhang, H. B. Wu, S. Madhavi, H. H. Hng, X. W. Lou, *J. Am. Chem. Soc.* **2012**, *134*, 17388–17391.
[14] Y.-M. Lin, P. R. Abel, A. Heller, C. B. Mullins, *J. Phys. Chem. Lett.* **2011**, *2*, 2885–2891.
[15] M. V. Reddy, T. Yu, C. H. Sow, Z. X. Shen, C. T. Lim, G. V. Subba Rao, B. V. R. Chowdari, *Adv. Funct. Mater.* **2007**, *17*, 2792–2799.
[16] a) Z. Zhang, C. Fang, J. Muhammad, J. Liang, W. Yang, X. Zhang, Z. Rong, X. Guo, Y. Jung, X. Dong, *Ionics* **2021**, *27*, 2431–2444; b) G. Backert, B. Oschmann, M. N. Tahir, F. Mueller, I. Lieberwirth, B. Balke, W. Tremel, S. Passerini, R. Zentel, *J. Colloid Interface Sci.* **2016**, *478*, 155–163; c) N. Zhang, X. Han, Y. Liu, X. Hu, Q. Zhao, J. Chen, *Adv. Energy Mater.* **2015**, *5*, 1401123; d) B. Liu, Q. Zhang, Z. Jin, L. Zhang, L. Li, Z. Gao, C. Wang, H. Xie, Z. Su, *Adv. Energy Mater.* **2018**, *8*, 1702347.
[17] a) L. H. Heß, A. Balducci, *ChemSusChem* **2018**, *11*, 1919–1926; b) L. Köps, C. Leibing, L. H. Hess, A. Balducci, *J. Electrochem. Soc.* **2021**, *168*, 010513; c) J. Atik, S. Röser, R. Wagner, D. Berghus, M. Winter, I. Cekic-Laskovic, *J. Electrochem. Soc.* **2020**, *167*, 040509; d) L. H. Hess, S. Wankmüller, L. Köps, A. Bothe, A. Balducci, *Batteries & Supercaps* **2019**, *2*, 852–857; e) C. Leibing, A. Balducci, *J. Electrochem. Soc.* **2021**, *168*, 090533.
[18] a) L. Medenbach, L. C. Meyer, A. Balducci, *Electrochem. Commun.* **2021**, *125*, 107001; b) S. Liu, L. C. Meyer, L. Medenbach, A. Balducci, *Energy Storage Mater.* **2022**, *47*, 534–541.
[19] K. L. Parry, A. G. Shard, R. D. Short, R. G. White, J. D. Whittle, A. Wright, *Surf. Interface Anal.* **2006**, *38*, 1497–1504.
[20] S. Menne, T. Vogl, A. Balducci, *Chem. Commun.* **2015**, *51*, 3656–3659.
[21] a) Y. Xiao, S. H. Lee, Y.-K. Sun, *Adv. Energy Mater.* **2017**, *7*, 1601329; b) J. Ye, D. Zhao, Q. Hao, C. Xu, *Electrochim. Acta* **2016**, *222*, 1402–1409; c) W. Wei, S. Yang, H. Zhou, I. Lieberwirth, X. Feng, K. Müllen, *Adv. Mater.* **2013**, *25*, 2909–2914; d) F. Zheng, Z. Yin, H. Xia, Y. Zhang, *Mater. Lett.* **2017**, *197*, 188–191; e) G. Li, Y. Li, J. Chen, P. Zhao, D. Li, Y. Dong, L. Zhang, *Electrochim. Acta* **2017**, *245*, 941–948; f) F. Zheng, Z. Yin, H. Xia, G. Bai, Y. Zhang, *Chem. Eng. J.* **2017**, *327*, 474–480; g) Z. Cai, L. Xu, M. Yan, C. Han, L. He, K. M. Hercule, C. Niu, Z. Yuan, W. Xu, L. Qu, K. Zhao, L. Mai, *Nano Lett.* **2015**, *15*, 738–744; h) F. Ma, A. Yuan, J. Xu, *ACS Appl. Mater. Interfaces* **2014**, *6*, 18129–18138; i) A. Brandt, F. Winter, S. Klamor, F. Berkemeier, J. Rana, R. Pöttgen, A. Balducci, *J. Mater. Chem. A* **2013**, *1*, 11229–11236.
[22] a) Z. Zhao, G. Tian, A. Sarapulova, V. Trouillet, Q. Fu, U. Geckle, H. Ehrenberg, S. Dsoke, *J. Mater. Chem. A* **2018**, *6*, 19381–19392; b) S. Laruelle, S. Grugeon, P. Poizot, M. Dolle, L. Dupont, J. Tarascon, *J. Electrochem. Soc.* **2002**, *149*, A627.
[23] a) L. El Ouatani, R. Dedryvère, C. Siret, P. Biensan, S. Reynaud, P. Iratçabal, D. Gonbeau, *J. Electrochem. Soc.* **2009**, *156*, A103; b) R. Stockhausen, A. Hofmann, L. Gehrlein, T. Bergfeldt, M. Müller, H. Ehrenberg, A. Smith, *J. Electrochem. Soc.* **2021**, *168*, 080504.

Manuscript received: March 31, 2022
Revised manuscript received: April 29, 2022
Accepted manuscript online: May 5, 2022
Version of record online: May 24, 2022